UDK/*UDC*: ##########
Izvirni znanstveni članek – *Original scientific paper*
DOI: 10.15292/acta.hydro.2026.05

Prejeto/*Received:* 21.06.2026
Sprejeto/*Accepted:* xx.xx.xxxx
Objavljeno na spletu/*Published online:* 16.11.2026

WAVE TRANSMISSION PERFORMANCE OF A SUBMERGED BREAKWATER CONSTRUCTED FROM ARTIFICIAL REEF BRICK-2 (ARB-2): PHYSICAL MODEL EXPERIMENTS AND NON-DIMENSIONAL ANALYSIS

PREPUSTNOST POTOPOLJENEGA VALOBRANA IZ UMETNIH GREBENSKIH OPEK (ARB-2) ZA VALOVE: FIZIKALNI MODELSKI EKSPERIMENTI IN BREZDIMENZIJSKA ANALIZA

Andrew Ghea Mahardika[1], S. Imam Wahyudi[2], Rachmat Mudiyono[3]

[123]Civil Engineering Study Program, Faculty of Engineering, Sultan Agung Islamic University, Semarang, INDONESIA

Abstract

Submerged breakwaters have gained increasing attention as coastal protection measures that attenuate incident wave energy while preserving ecological connectivity and visual landscape integrity. The Artificial Reef Brick-2 (ARB-2) is a modular, perforated concrete unit engineered to combine wave dissipation with artificial reef functionality. This study aims to experimentally quantify the wave transmission performance of an ARB-2 submerged breakwater model and to identify the non-dimensional parameters governing its transmission coefficient (*Kt*). Physical model experiments were conducted in a laboratory wave flume equipped with a piston-type wave generator. Two capacitive wave gauges recorded incident and transmitted wave heights, which were analyzed using the zero-crossing method. Water depth, wave height, wave period, and crest submergence depth were systematically varied across 90 experimental runs. Wavelength was computed iteratively from the linear wave theory dispersion relation. The transmission coefficient ranged from 0.175 to 0.469, with structural geometry – specifically relative submergence (*Rc*/*Hi*) and relative crest width (*B*/*L*) – exerting the strongest influence on *Kt*. Power-law regression yielded exponents of −0.069, +0.2832, and −0.130 for wave steepness, relative submergence, and relative crest width, respectively. The ARB-2 module consistently reduces transmitted wave heights through overtopping turbulence, internal pore friction, and vortex generation, confirming its suitability as an eco-compatible coastal protection structure. This study provides the first empirical non-dimensional characterization of wave transmission through ARB-2, establishing validated applicability ranges for practical design application.

Keywords: wave transmission; submerged breakwater; Artificial Reef Brick-2; coastal protection; physical modeling; non-dimensional analysis.

Izvleček

[1] Stik / *Correspondence*: andrewgheamahardika@gmail.com

© Mahardika A. G.. et al.; This is an open-access article distributed under the terms of the Attribution-ShareAlike 4.0 International (CC BY-SA 4.0) licence.

© Mahardika A. G. et al.; Vsebina tega članka se sme uporabljati v skladu s pogoji licence Priznanje avtorstva-Deljenje pod enakimi pogoji 4.0 Mednarodna (CC BY-SA 4.0).

Potopljeni valobrani so deležni vse večje pozornosti kot ukrepi za zaščito obale, saj zmanjšujejo energijo vpadnih valov, hkrati pa ohranjajo ekološko povezanost in vizualno celovitost krajine. Umetna grebenska opeka (ARB-2) je modularni, perforirani betonski element, ki združuje dušenje valov s funkcionalnostjo umetnih podvodnih grebenov. Cilj te raziskave je eksperimentalno kvantificirati prepustnost za valove modela potopljenega valobrana ARB-2 in določiti brezdimenzijske parametre, ki vplivajo na koeficient prepustnosti (*Kt*). Fizikalni modelski eksperimenti so bili izvedeni v laboratorijskem valovnem kanalu z generatorjem valov. Dva kapacitivna merilnika valov sta beležila višine vpadnih in prepuščenih valov, ki so bili analizirani z metodo prehoda skozi nič. Globina vode, višina valov, perioda valov in globina potopljenosti grebena so bile sistematično spreminjane v 90 eksperimentalnih preizkusih. Valovna dolžina je bila iterativno izračunana z disperzijsko relacijo linearne teorije valov. Koeficient prepustnosti se je gibal od 0,175 do 0,469, pri čemer je imela strukturna geometrija – zlasti relativni nadvišek (*Rc*/*Hi*) in relativna širina grebena (*B*/*L*) – najmočnejši vpliv na *Kt*. Modul ARB-2 dosledno zmanjšuje višine prepuščenih valov s turbulenco ob prelivanju, trenjsko silo v porah in generiranjem vrtincev, kar potrjuje njegovo ustreznost kot ekološko sprejemljivo konstrukcijo za zaščito obale.

Ključne besede: prepustnost za valove, potopljeni valobran, umetna grebenska opeka (ARB-2), zaščita obale, fizikalno modeliranje, brezdimenzijska analiza

1. Introduction

Coastal zones, where natural hydrodynamic processes interact continuously with anthropogenic activities and land use change, are some of the most dynamic and ecologically sensitive environments on Earth. Progressive shoreline retreat, beach erosion, nearshore infrastructure damage, and marine habitat degradation are widely reported consequences of sustained wave energy impingement, storm surges, and tidal fluctuations (Wahyudi and Adi, 2018). These pressures are further compounded by accelerating climate change, which drives sea-level rise, increases storm frequency and intensity, and broadens the geographic extent of coastal hazards. In this context, the demand for effective, sustainable, and ecologically compatible coastal protection systems has reached critical importance.

Conventional coastal defense structures – including seawalls, revetments, and emerged breakwaters – have demonstrated effectiveness in protecting backshore areas from direct wave attacks. However, their rigid, opaque geometry produces well-documented adverse secondary effects: disruption of longshore sediment transport, erosion at the structure toe, reduction of beach width and recreational value, and degradation of nearshore benthic habitats (Wahyudi et al., 2012). As recognition of these limitations has grown, research attention has shifted toward structures that attenuate wave energy while minimizing physical and ecological disruption. Submerged low-crested structures, positioned partially or entirely beneath the still water level, have emerged as a promising class of such alternatives (Magdalena et al., 2020; Repousis et al., 2023).

A submerged breakwater functions by intercepting propagating waves at depth, inducing turbulence, partial breaking, and energy redistribution as the wave column interacts with the structure crest and body (Min et al., 2023). Unlike emerged structures, submerged units do not create a complete barrier to water circulation and can support greater habitat connectivity between inshore and offshore zones than impermeable emerged structures; however, the extent of any associated cross-structure sediment exchange is site- and design-specific and should not be generalized without direct evidence. This characteristic makes them attractive for deployment in areas where both coastal protection and marine ecosystem preservation are management priorities. Their hydrodynamic performance is governed by a set of interdependent parameters including crest elevation relative to the still water level (*Rc*), incident wave height (*Hi*), wave period (*T*), structure width (*B*), and wavelength (*L*) (Huddiankuwera et al., 2024; Haz et al., 2022).

In parallel with the development of submerged breakwaters, artificial reef technology has grown substantially as a field, combining engineering and ecological objectives. Artificial reef modules are designed to replicate the structural complexity of natural coral reefs or rocky seabeds, providing substrates for colonization by marine organisms while simultaneously delivering hydrodynamic functions (Adi et al., 2020). The integration of these two concepts – submerged coastal protection and artificial reef design – has motivated the development of hybrid modular units such as the Artificial Reef Brick (ARB) series. The Artificial Reef Brick-2 (ARB-2) is an evolution of this concept: a perforated concrete block with multiple internal cylindrical cavities designed to maximize pore-scale turbulence and flow resistance while maintaining structural interlocking capacity. Its stepped assembly configuration enables the construction of a trapezoidal submerged mound geometry, which promotes gradual wave interaction across the structure width.

Wave transmission through porous submerged structures has been investigated through a combination of physical experiments, numerical simulations, and analytical formulations. Magdalena et al. (2020) provided mathematical solutions for wave transmission by rectangular submerged breakwaters, demonstrating that freeboard ratio and wavelength are the dominant parameters. Repousis et al. (2023) conducted large-scale experiments on rubble-mound submerged breakwaters, deriving semi-empirical prediction equations applicable to a wide range of wave conditions. Min et al. (2023) numerically investigated dual porous submerged breakwaters using a fully nonlinear numerical wave tank, revealing complex nonlinear wave-porous medium interactions that significantly influence the transmission coefficient. Silva et al. (2024) extended this understanding to the laboratory scale, analyzing wave-driven hydrodynamics over submerged coastal structures in a two-dimensional wave basin to characterize energy transformation patterns above artificial reef geometries.

Research specifically addressing Indonesian coastal environments has highlighted the relevance of submerged structures for nearshore protection, given the high wave energy climate and extensive shallow reef systems along the archipelago coastline. Azima et al. (2023) evaluated the effectiveness of emerged and submerged breakwaters at Tanjung Medang Beach, demonstrating measurable wave height reduction at sites with moderate submergence depths. Suprijo et al. (2024) examined wave transformation produced by staggered pile breakwaters, confirming that structure configuration and spacing significantly modify regular wave propagation. Rachmanda et al. (2022) performed stability analyses on submerged rock breakwaters, providing insight into the coupling between structural integrity and hydrodynamic performance. Huddiankuwera et al. (2024) specifically investigated the influence of wave parameters on transmission coefficients for hollow submerged breakwaters, identifying geometric ratios as dominant predictors consistent with the broader international literature.

The experimental and numerical body of literature on submerged porous structures has converged around the use of non-dimensional parameter groups to characterize transmission performance in a scalable, geometry-independent manner. Mahardika and Ramady (2020) demonstrated that, for artificial reef brick configurations, non-dimensional variables such as wave steepness, relative crest elevation, and relative structure width provided meaningful correlations with measured transmission coefficients. However, their work focused on the first ARB generation (ARB-1) and did not extend the analysis to the ARB-2 unit, which features a different cavity geometry, porosity arrangement, and assembly strategy.

Despite the expanding knowledge base on submerged porous breakwaters, critical gaps remain that constrain the direct application of existing literature to ARB-2 design. First, no empirical study has quantified the non-dimensional transmission behavior of the ARB-2 module under systematic variation of wave period, height, and submergence in a controlled flume setting. Second, the combined influence of multiple geometric and wave parameters on Kt has not been formulated as a power-law predictive model for this specific unit

type. Third, validated applicability ranges for non-dimensional design variables have not been established for ARB-2, limiting the transfer of experimental findings to field-scale applications. The present study addresses these gaps directly.

The principal objectives of this study are: (1) to experimentally measure the wave transmission coefficient (*Kt*) of an ARB-2 submerged breakwater model over a systematically varied range of wave and structural conditions; (2) to identify the relative influence of three non-dimensional parameters – wave steepness (Hi/gT^2), relative submergence (Rc/Hi), and relative crest width (B/L) – on transmission performance; and (3) to derive and validate a power-law regression model for *Kt* with defined applicability limits. The scientific contribution of this work lies in providing the first experimentally validated, non-dimensionally parameterized characterization of the ARB-2 as a submerged breakwater, establishing a quantitative design basis for its application in coastal engineering practice.

2. Literature Review

2.1 Submerged Breakwaters and Wave Attenuation Mechanisms

The hydrodynamic behavior of submerged breakwaters has been studied extensively through laboratory experimentation, analytical theory, and numerical simulation. A submerged structure modifies the propagation of surface gravity waves through three primary mechanisms: partial wave breaking at the crest, turbulence generation within and above the structure, and partial reflection of incident energy back toward the wave generator (Magdalena et al., 2020). The relative magnitude of these mechanisms depends strongly on the degree of submergence, expressed as the ratio of crest depth to incident wave height (Rc/Hi). Shallowly submerged crests promote wave breaking and overtopping turbulence, whereas deeply submerged structures primarily induce pore-scale energy dissipation and sub-surface reflection (Repousis *et al.*, 2023). The transmission coefficient ($Kt = Ht/Hi$), defined as the ratio of transmitted to incident wave height, quantifies the net efficiency of this attenuation and is the primary performance metric in both design and evaluation contexts (Haz et al., 2022).

Repousis et al. (2023) conducted extensive experiments on rubble-mound submerged breakwaters subjected to irregular wave spectra, deriving semi-empirical prediction equations based on crest freeboard (*Rc*), incident significant wave height (*Hs*), and spectral peak period (*Tp*). Their results confirmed that Rc/Hs is the dominant predictor of *Kt*, accounting for more variance than structure width or slope. Magdalena et al. (2020) derived closed-form analytical solutions for rectangular submerged breakwaters under linear wave theory, demonstrating that dimensionless transmission depends primarily on the ratio of freeboard to incident wavelength.

Several studies established the empirical and semi-empirical basis that later work, including the present study, builds on. d'Angremond, van der Meer, and de Jong (1997) proposed one of the first widely used transmission formulae for low-crested structures, expressing Kt primarily as a function of relative crest freeboard and structure slope; the formula performs well for rubble-mound sections but was calibrated on relatively narrow-crested, non-porous geometries. Calabrese, Vicinanza, and Buccino (2003) extended this basis with large-scale experiments on low-crested and submerged breakwaters under broken-wave conditions, showing that wave breaking upstream of the structure can substantially modify transmission relative to the unbroken-wave case, a mechanism not captured by purely geometric formulae. Goda and Ahrens (2009) reformulated wave transmission over and through low-crested structures using a unified framework that separates overtopping and through-structure transmission, improving applicability to porous designs but requiring more input parameters than simpler freeboard-based formulae. Tomasicchio and D'Alessandro (2013) compared several existing transmission formulae against a common dataset and found that predictive accuracy varies considerably with structure porosity and relative submergence, with errors that can exceed 20–30% outside the calibration range of a given formula – underscoring the importance of

reporting the applicability range explicitly, as done in Table 3 of the present study. Kurdistani, Tomasicchio, D'Alessandro, and Francone (2022) developed a transmission formula specific to submerged homogeneous porous breakwaters, reporting prediction errors on the order of 10–15% within their calibration dataset; because their structures are porous and submerged, this formula is the most directly comparable precedent to ARB-2 among the studies reviewed here, although differences in unit geometry (homogeneous porous mound versus discrete cavitied blocks) limit direct numerical comparison. Taken together, this body of work indicates that formulae calibrated on solid or homogeneous porous rubble-mound sections do not necessarily transfer to modular, cavitied block structures such as ARB-2 without re-calibration, which motivates the site- and structure-specific regression developed in Section 4.

2.2 Porous and Artificial Reef Structures

Porous submerged structures introduce additional energy dissipation through internal flow resistance, viscous friction, and inertia forces within the pore space. Min et al. (2023) employed a fully nonlinear numerical wave tank with an embedded porous domain to simulate wave interaction with dual porous submerged breakwaters. Their simulations demonstrated that pore resistance parameters – including the Forchheimer friction coefficient and porosity – directly control the energy dissipation efficiency and the shape of the transmitted wave spectrum. Under intermediate-water wave conditions, porous resistance was found to produce transmission coefficients approximately 15–25% lower than those predicted for equivalent impermeable structures, underscoring the engineering advantage of porous unit designs.

Artificial reef structures extend the functionality of porous submerged breakwaters by incorporating geometric complexity that mimics natural reef topography. Silva et al. (2024) investigated wave-driven hydrodynamics over submerged coastal structures and artificial reefs in a laboratory wave basin, demonstrating complex energy transformation patterns attributable to the three-dimensional nature of reef topology. Rudan (2024) evaluated the influence of structure topology and position on submerged breakwater efficiency, confirming that multi-layered configurations consistently outperform single-layer designs through enhanced dissipation over a larger structure volume.

The ARB series – including both the first-generation Artificial Reef Brick and the newer ARB-2 variant – was developed as a modular artificial reef unit combining coastal protection capability with ecological habitat value (Adi et al., 2020). The ARB-2 features cylindrical internal cavities of varying diameters on each face, producing a high-porosity, complex-geometry block. Mahardika and Ramady (2020) conducted the first reported laboratory study on artificial reef brick configurations, demonstrating that Kt for these modular units is governed by wave steepness, relative crest width, and relative submergence, consistent with the broader literature on submerged porous breakwaters.

2.3 Non-Dimensional Framework for Transmission Prediction

The use of non-dimensional parameter groups to characterize wave transmission is well established in the coastal engineering literature, enabling experimental results to be scaled to prototype conditions and compared across studies employing various structural scales and wave climates. The three groups most consistently identified as predictors of Kt for submerged breakwaters are: (1) wave steepness (Hi/gT^2 or Hi/L), which describes the incident wave shape and its tendency to break; (2) relative submergence (Rc/Hi), which captures the interaction between submergence depth and incident wave amplitude; and (3) relative structure width (B/L), which quantifies the spatial extent of wave–structure interaction relative to the incident wavelength (Huddiankuwera et al., 2024; Haz et al., 2022).

Power-law regression models of the form $Kt = a \cdot (Hi/gT^2)^{n_1} \cdot (Rc/Hi)^{n_2} \cdot (B/L)^{n_3}$ have been successfully applied in the literature to synthesize multi-variable experimental datasets into compact, interpretable prediction formulae. This functional form captures

the multiplicative interaction of wave and geometric parameters and provides a direct basis for sensitivity analysis through the magnitudes and signs of the exponents (Mahardika and Ramady, 2020). This framework is adopted in the present study to characterize ARB-2 performance and to enable direct comparison with results from prior investigations.

2.4 Conceptual Synthesis and Research Gap

A synthesis of the reviewed literature confirms that submerged porous breakwaters, including modular artificial reef units, serve as an effective and ecologically compatible coastal protection strategy. The evidence base for conventional rubble-mound and rectangular submerged breakwaters is well developed, with multiple validated prediction formulae available for engineering design. However, the literature on specifically modular, highly porous concrete units with cylindrical cavity geometry – the category to which ARB-2 belongs – remains limited. Existing studies on first-generation ARB configurations did not establish validated non-dimensional applicability ranges, and no multi-variable power-law model for ARB-2 has been reported. This gap between the demonstrated hydrodynamic potential of the ARB-2 system and the absence of quantified, validated design parameters constitutes the primary motivation for the present experimental investigation.

3. Methods

3.1 Research Design

This study adopted a quantitative experimental research design employing physical hydraulic modeling to investigate wave transmission through the ARB-2 submerged breakwater. The methodological approach aligns with established practice in coastal hydraulic engineering, in which laboratory wave flume experiments provide controlled, repeatable conditions for measurement of incident and transmitted wave characteristics. The physical model serves as the principal source of empirical data, with dimensional analysis and non-dimensional regression applied in post-processing to derive scalable prediction relationships. Table 1 summarizes the full parameter set and their experimental ranges.

3.2 Physical Model Configuration

The experiments were conducted in a glass-walled laboratory wave flume equipped with a piston-type wave generator capable of producing regular monochromatic waves with controlled height and period settings. The ARB-2 units were fabricated from perforated concrete and featured multiple cylindrical internal cavities of various diameters on each face, creating a high-porosity block geometry. Individual units were assembled in a stepped pyramidal configuration to form a continuous submerged structure spanning the full cross-sectional width of the flume. The stepped geometry promotes progressive wave interaction across multiple elevation layers as the wave propagates over the structure, improving turbulence generation and energy dissipation compared to a flat-crested arrangement.

To prevent displacement under repeated wave loading, all ARB-2 units were mechanically interlocked after final positioning was confirmed. This locking mechanism ensured rigid boundary conditions throughout the testing program, isolating hydrodynamic behavior from any confounding influence of structural movement. The resulting configuration maintained a consistent crest elevation and cross-sectional geometry across all trials. Figure 2 illustrates the three-dimensional prototype configuration of the ARB-2 assembly, while Figure 3 shows the submerged model in the wave flume at operating water depth.

The flume is a glass-walled, open channel measuring 17.5 m long, 0.30 m wide, and 0.50 m high. The upstream capacitive wave gauge was positioned at $x \approx 8.0$ m (approximately 1.0 m upstream of the ARB-2 structure toe), and the downstream capacitive wave gauge at $x \approx 12.1$ m (approximately 1.6 m downstream of the structure toe); both channels were sampled at 50 Hz. Wave energy at the far end of the flume was dissipated by a passive artificial beach (no active absorption system), beginning at approximately $x = 13.5$ m. The physical model was scaled at an approximate

Froude length scale of 1:10 ($\lambda L = 10$, $\lambda T = \sqrt{10}$); Froude similarity preserves gravity-wave kinematics but not Reynolds similarity, so viscous- and pore-scale dissipation processes within the ARB-2 cavities may be subject to scale effects that should be considered when extrapolating results to prototype scale.

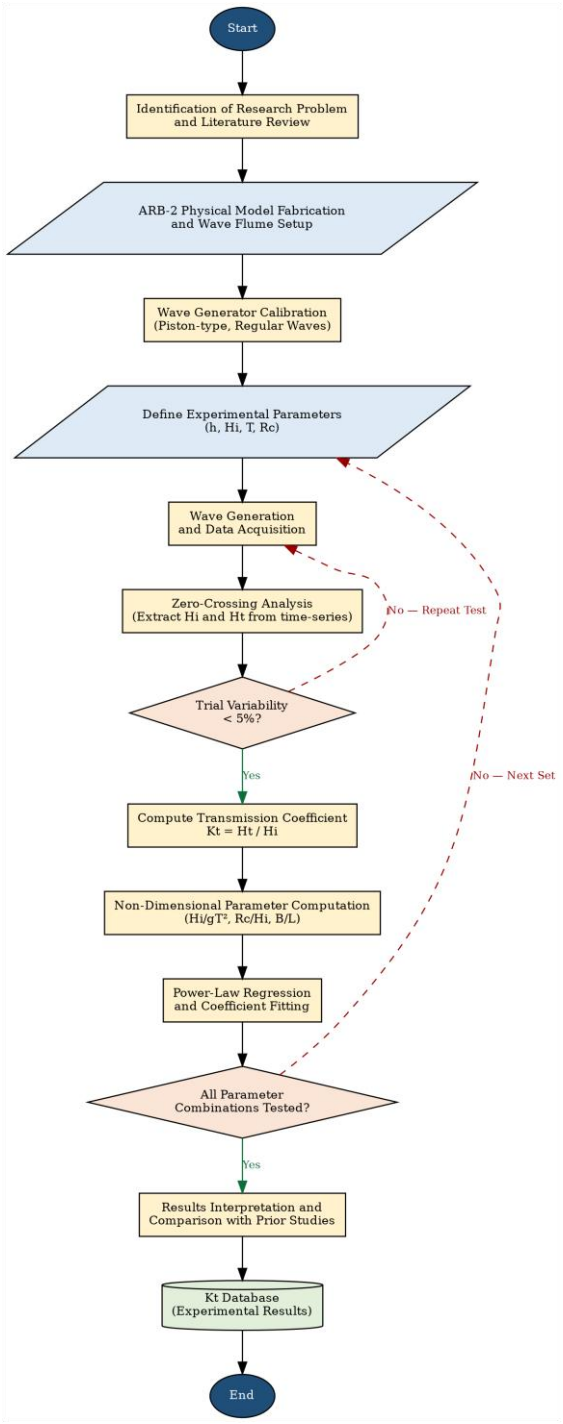


***Figure 1**: Research flowchart illustrating the methodological sequence for the ARB-2 wave transmission experiment, including wave generation, data acquisition, analysis, and regression. Source: authors' elaboration.*

***Slika 1**: Diagram poteka raziskave, ki prikazuje metodološko zaporedje za eksperiment prepustnosti za valove ARB-2, vključno z generiranjem valov, zajemanjem podatkov, analizo in regresijo.*

***Table 1**: Summary of experimental parameters and their ranges.*

***Preglednica 1**: Povzetek eksperimentalnih parametrov in njihovih obsegov.*

No.	Parameter	Symbol	Range	Unit
1	Water depth	*h*	0.25–0.40	m
2	Incident wave height	*Hi*	0.030–0.100	m
3	Wave period	*T*	1.0–2.5	s
4	Crest submergence depth	*Rc*	0.010–0.080	m
5	Wavelength (computed)	*L*	1.30–4.74	m
6	Structure crest width	*B*	0.20–0.35	m
7	Transmission coefficient	*Kt*	0.175–0.469	–

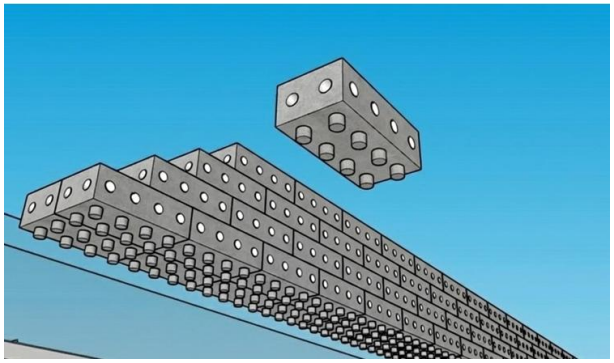


***Figure 2:** Three-dimensional prototype configuration of the Artificial Reef Brick-2 (ARB-2) modular assembly, showing the stepped arrangement and perforated face geometry. Source: authors' elaboration (laboratory prototype, Sultan Agung Islamic University).*

***Slika 2:** Tridimenzionalna prototipna konfiguracija modularnega sklopa umetne grebenske opeke (ARB-2), ki prikazuje stopničasto razporeditev in perforirano geometrijo čelne ploskve.*



***Figure 3:** ARB-2 submerged breakwater model installed in the wave flume at operating water depth, showing the pyramidal stepped configuration and submerged condition. Source: authors' elaboration (laboratory wave flume experiment).*

***Slika 3:** Model potopljenega valobrana ARB-2, nameščen v valovnem kanalu pri obratovalni globini vode, ki prikazuje piramidalno stopničasto konfiguracijo in potopljeno stanje.*

3.3 Instrumentation and Data Collection

Two capacitive wave gauges were deployed inside the flume to record incident and transmitted wave heights. The upstream gauge, positioned between the wave generator and the ARB-2 structure, measured the incident wave height (*Hi*), while the downstream gauge recorded the transmitted wave height (*Ht*) after the wave had passed over and through the structure. Gauge spacing and placement followed established laboratory guidelines for minimizing contamination from re-reflected waves, secondary interactions, and evanescent modes. Sampling rates were set at 50 Hz to ensure adequate temporal resolution for all wave periods tested. Time-series records were processed using the zero-crossing method, which identifies successive upward zero crossings in the surface elevation signal to delineate individual wave cycles, from which mean crest-to-trough wave heights were extracted.

Water depth, incident wave height, wave period, and crest submergence depth were varied systematically across the experimental program to generate a representative range of hydrodynamic conditions. For each combination of parameters, a minimum of three independent repeat runs was conducted. Any set of repeated trials exhibiting inter-run variability exceeding 5% was discarded and replaced with a new set of measurements to maintain data quality. Wavelength (*L*) for each

wave period and water depth was computed iteratively using the linear wave theory dispersion relation:

$$L = \left(\frac{gT^2}{2\pi}\right)\tanh\left(\frac{2\pi h}{L}\right) \quad (1)$$

where g is gravitational acceleration (9.81 m/s²), T is the wave period (s), h is the still water depth (m), and L is the wavelength (m). Newton–Raphson iteration was applied to solve for L to a convergence tolerance of 10^{-6} m.

3.4 Computation of Transmission Coefficient

The transmission coefficient (*Kt*) was calculated as:

$$K_t = \frac{H_t}{H_i} \quad (2)$$

where *Ht* is the mean transmitted wave height measured downstream of the structure and *Hi* is the mean incident wave height measured upstream. A value of *Kt* = 1 indicates complete transmission (zero attenuation), while *Kt* = 0 indicates complete energy dissipation. Intermediate values represent partial attenuation, with lower values corresponding to superior structure performance.

3.5 Non-Dimensional Analysis and Regression

Following computation of *Kt* for all experimental runs, three non-dimensional parameter groups were derived: (1) wave steepness (Hi/gT^2), (2) relative submergence (Rc/Hi), and (3) relative crest width (B/L), where *Rc* is the crest submergence depth and *B* is the structure crest width. A power-law regression of the form:

$$K_t = a\left(\frac{H_i}{gT^2}\right)^{n_1}\left(\frac{R_c}{H_i}\right)^{n_2}\left(\frac{B}{L}\right)^{n_3} \quad (3)$$

was fitted to the full experimental dataset by log-linearization, followed by least-squares regression. Coefficients (a) and exponents (n_1, n_2, n_3) were extracted for each variable, and the validity ranges of each non-dimensional group were documented to define the applicability limits of the derived model.

4. Results and Discussion

4.1 Overview of Experimental Results

The experimental program generated a comprehensive dataset covering 90 individual test runs distributed across the full parameter space defined in the methodology. Incident wave heights recorded by the upstream gauge exhibited stability across all trials, with standard deviations consistently below 3% of the mean value for each test set, confirming that the wave generator produced reliable and repeatable input conditions. The transmitted wave height downstream of the ARB-2 structure varied more strongly across the 90 runs than the incident wave height (coefficient of variation up to approximately 12% within repeated sets, versus under 1% for the incident signal), because transmission responds jointly to wave steepness, relative submergence, and relative crest width rather than to incident wave height alone.

Time-series records processed by the zero-crossing method consistently demonstrated a reduction in wave amplitude after interaction with the ARB-2 structure. The most pronounced attenuation occurred under conditions of short wave period and shallow crest submergence, consistent with the physical expectation that greater wave–structure interaction produces higher energy dissipation. The computed transmission coefficients ranged from a minimum of 0.175 to a maximum of 0.469 across the full dataset, spanning a dissipation range of 53.1% to 82.5% of incident wave height. Table 2 summarizes the regression coefficients and exponents derived from the non-dimensional analysis.

Table 2: *Regression coefficients and exponents for non-dimensional variables.*

Preglednica 2: *Regresijski koeficienti in eksponenti za brezdimenzijske spremenljivke.*

No.	Non-dimensional parameter	95% CI for n	Exponent (n)	Source
1	Hi/gT² (wave steepness)	−0.108 to −0.029	−0.069	Authors' elaboration
2	Rc/Hi (relative submergence)	0.248 to 0.317	+0.2832	Authors' elaboration
3	B/L (relative crest width)	−0.186 to −0.075	−0.130	Authors' elaboration

The full multivariable power-law model, fitted by ordinary least squares on log-transformed variables, is $K_t = a\left(\frac{H_i}{gT^2}\right)^{n_1}\left(\frac{R_c}{H_i}\right)^{n_2}\left(\frac{B}{L}\right)^{n_3}$, with a single global coefficient a = 0.1354 (95% CI: 0.113–0.162); the exponents n1, n2, and n3 are listed in Table 2. The model explains a large share of the observed variance (R^2 = 0.856, adjusted R^2 = 0.851, F(3,86) = 170.3, p < 0.001, N = 90). Applying the fitted coefficients to all 90 runs yields predicted Kt values with a root-mean-square error of 0.0227 and a standard deviation of the observed Kt of 0.0595, both computed directly from the full dataset (Table 3 reports the applicability ranges).

4.2 Influence of Non-Dimensional Parameters on Kt

Figure 4 presents scatter plots of the transmission coefficient against each of the three non-dimensional parameter groups. The left panel (Panel A) plots *Kt* against wave steepness (Hi/gT^2). Data points span a comparatively narrow band of steepness values (Hi/gT^2 from 0.00049 to 0.01019), a range determined by the wave heights and periods achievable in the flume; because this range is narrow relative to the spread in the other two non-dimensional groups, the steepness trend is less well resolved than the freeboard and crest-width trends. The fitted trend line confirms a weak negative relationship, indicated by the exponent of −0.069, meaning that higher wave steepness is marginally associated with lower transmission.

The central panel (Panel B) depicts the relationship between *Kt* and relative submergence (*Rc*/*Hi*). This parameter exhibits the widest spread in the experimental dataset and the strongest positive correlation with *Kt*, yielding an exponent of +0.2832. As *Rc*/*Hi* increases – corresponding to deeper structural submergence relative to incident wave height – the transmission coefficient rises systematically. The right panel (Panel C) shows the relationship between *Kt* and relative crest width (*B*/*L*), which exhibits a moderate negative correlation with an exponent of −0.130. These results collectively align with observations by Mahardika and Ramady (2020) and Haz et al. (2022), who identified geometric parameters as dominant controllers of transmission performance.

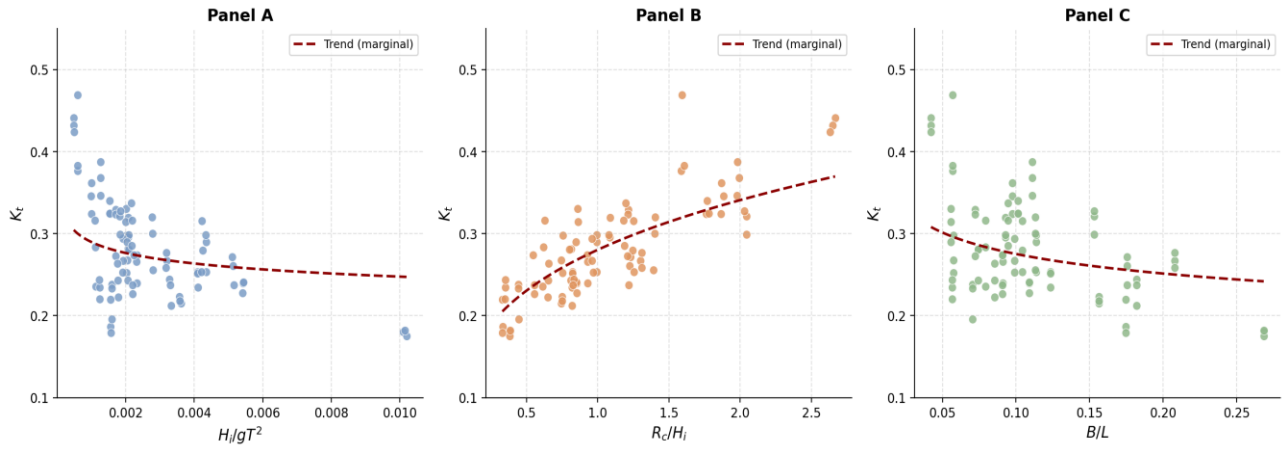


Figure 4: *Scatter plots of transmission coefficient (Kt) against three non-dimensional parameters: Panel A – wave steepness (Hi/gT²); Panel B – relative submergence (Rc/Hi); Panel C – relative crest width (B/L). Dashed red lines indicate marginal trend from power-law regression. Source: authors' elaboration based on wave flume experimental data.*

Slika 4: *Diagrami raztrosa koeficienta prepustnosti (Kt) v odvisnosti od treh brezdimenzijskih parametrov: A – strmina vala (Hi/gT²); B – relativno nadvišanje (Rc/Hi); C – relativna širina grebena (B/L). Prekinjena rdeča črta označuje mejni trend potenčne regresije.*

Table 3: *Applicability range of non-dimensional parameters.*

Preglednica 3: *Območje uporabnosti brezdimenzijskih parametrov.*

No.	Parameter	Minimum	Maximum	Source
1	Hi/gT^2	0.00049	0.01019	Authors' elaboration
2	Rc/Hi	0.331	2.667	Authors' elaboration
3	B/L	0.042	0.268	Authors' elaboration

4.3 Energy Dissipation Mechanisms

The mechanisms responsible for wave energy attenuation in the ARB-2 system can be identified through analysis of the transmitted wave profiles and the parameter sensitivity patterns observed in the experimental data. Table 4 provides a structured cross-comparison of the *Kt* ranges obtained in the present study with those reported in prior studies on submerged breakwaters and artificial reef structures.

The *Kt* range of 0.175–0.469 achieved by ARB-2 is lower than the ranges reported for rubble-mound and rectangular impermeable submerged breakwaters under their respective test conditions (Table 4), reported as *Kt* values of 0.36–0.99 (Repousis et al., 2023) and 0.824–1.086 (Magdalena et al., 2020). Table 4 also reports the wave type used by each comparator, since *Kt* values obtained under regular monochromatic waves (present study; Magdalena et al., 2020; Haz et al., 2022; Rachmanda et al., 2022) are not directly comparable to those obtained under irregular, spectrum-based sea states (Repousis et al., 2023, tested with both regular and random waves; van Gent et al., 2023, tested exclusively with JONSWAP irregular spectra). Van Gent et al. (2023) reported $Kt = 0.50–1.00$ for trapezoidal submerged structures and artificial reef units under irregular waves, a substantially higher range than ARB-2, reflecting both the irregular-wave sea state used and, in several of their tested configurations, comparatively lower porosity and internal flow resistance than the multi-cavity ARB-2 geometry. The lower minimum *Kt* achievable with ARB-2 reflects the additional dissipation contributed by pore-scale friction and vortex generation within the cylindrical cavities of the module. Table 5 presents the energy dissipation mechanisms identified in the ARB-2 system, organized by physical process and governing condition.

The dominant mechanism under shallow submergence conditions is overtopping turbulence. Under deeper submergence, when crests do not directly interact with the structural surface, internal pore friction and vortex generation within the cylindrical cavities become the primary dissipation pathways. This mode transition with increasing *Rc*/*Hi* explains the positive exponent on relative submergence in the regression model – higher *Rc*/*Hi* implies deeper submergence, where the less efficient internal dissipation mechanisms dominate and *Kt* rises accordingly.

4.4 Influence of Wave Period on Transmission

Wave period exerts an indirect but significant influence on *Kt* through its effect on wavelength and, consequently, on relative crest width (*B*/*L*). Longer wave periods produce greater wavelengths, reducing *B*/*L* for a fixed structure width and increasing *Kt* in accordance with the negative exponent on this parameter. Shorter-period waves experience stronger curvature over the structure crest, facilitating more intensive breaking and turbulence. This period-dependent behavior is consistent with documented trends for submerged porous structures (Rudan, 2024; Min et al., 2023) and supports the engineering design principle that ARB-2 deployments in short-period wave environments will achieve the highest attenuation efficiency.

Table 4: *Comparison of transmission coefficient ranges across selected studies.*

Preglednica 4: *Primerjava razponov koeficienta prepustnosti v izbranih študijah.*

Study	Structure type	Wave type	Kt range	Key parameter	Source
Present study (ARB-2)	Modular porous artificial reef	Regular (monochromatic)	0.175–0.469	Rc/Hi, B/L	Authors' elaboration
Magdalena et al. (2020)	Rectangular submerged breakwater	Regular (monochromatic)	0.824–1.086	Freeboard ratio; note Kt>1 reported in some cases	Magdalena et al. (2020)
Repousis et al. (2023)	Rubble-mound submerged	Regular & irregular (random)	0.36–0.99	Crest freeboard, wave breaking type	Repousis et al. (2023)
Min et al. (2023)	Dual porous submerged	Regular (numerical)	0.15–0.75	Porosity, submergence	Min et al. (2023)
Haz et al. (2022)	Submerged with wavelength variation	Regular (monochromatic)	0.25–0.80	B/L, wave steepness	Haz et al. (2022)
van Gent et al. (2023)	Trapezoidal impermeable, permeable & perforated submerged	Irregular (JONSWAP spectrum)	0.50–1.00	Rc/Hi, relative crest width Gc/L	van Gent et al. (2023)
Rachmanda et al. (2022)	Submerged rock breakwater	Regular (physical model)	0.30–0.75	D50, crest width	Rachmanda et al. (2022)

Table 5: *Energy dissipation mechanisms in ARB-2 submerged breakwater.*

Preglednica 5: *Mehanizmi disipacije energije v potopljenem valobranu ARB-2.*

Mechanism	Physical description	Governing condition
Turbulence induced by overtopping and breaking	Wave crests overtop the submerged crest, producing surface rollers and turbulent shear layers that dissipate kinetic energy	Low Rc/h; shallow submergence; steep incident waves
Internal pore friction	Flow penetrating the ARB-2 internal cavities experiences viscous and form drag, converting wave energy into heat	High porosity; long wave period; moderate Hi/L
Vortex generation	Flow separation at module edges and cavity openings produces coherent vortices that absorb and scatter wave energy	Sharp-edged geometry; high incident velocity; $Re > 10^3$

Flow separation and re-attachment	Boundary layer separation at the upstream face of each layer creates drag forces that retard transmission	Multi-layer stack; strong velocity gradients
Partial reflection	A fraction of incident wave energy is reflected upstream by the stepped crest, reducing energy available for transmission	Wide B/L; steep crest profile

Table 6: *Key dimensional and non-dimensional parameters governing wave transmission in ARB-2.*

Preglednica 6: *Ključni dimenzijski in brezdimenzijski parametri, ki vplivajo na prepustnost za valove v ARB-2.*

Parameter category	**Variable**	**Effect on Kt**	**Source**
Wave	*Hi*	Higher Hi slightly increases Kt due to momentum dominance	Authors' elaboration
Wave	*T*	Longer T → higher Kt; shorter T → lower Kt	Mahardika & Ramady (2020)
Wave	Hi/gT^2	Weak influence under tested range	Authors' elaboration
Geometry	*Rc*	Shallower Rc → lower Kt; deeper Rc → higher Kt	Huddiankuwera et al. (2024)
Geometry	*B*	Wider B → lower Kt; wider B/L → increased dissipation	Haz et al. (2022)
Structure	Porosity	Higher porosity → more internal friction and vortex generation	Min et al. (2023)

4.5 Regression Model Validation and Figure Analysis

Figure 5 presents the signed exponents (n1, n2, n3) of the fitted multivariable power-law model, together with their 95% confidence intervals; the model has a single global coefficient a = 0.1354 (95% CI: 0.113–0.162). Relative submergence (Rc/Hi) has the largest-magnitude and most reliable exponent (n2 = +0.2832, 95% CI: 0.248–0.317), confirming it as the dominant control on Kt. Relative crest width (B/L) has an intermediate, negative exponent (n3 = −0.130, 95% CI: −0.186 to −0.075). Wave steepness (Hi/gT^2) has the smallest-magnitude exponent (n1 = −0.069, 95% CI: −0.108 to −0.029) and, correspondingly, the widest relative confidence interval, consistent with the narrow steepness range sampled in the flume.

Substitution of the fitted coefficients and exponents from Table 2 into equation (3) for all 90 experimental data points yielded predicted *Kt* values that fell within the measured range of 0.175–0.469, with a root-mean-square prediction error of 0.0227 (standard deviation of observed *Kt* of 0.0595) and a coefficient of determination of $R^2 = 0.856$ (adjusted $R^2 = 0.851$). This level of accuracy is consistent with prediction uncertainties reported for comparable empirical models in the literature (Repousis et al., 2023; Magdalena et al., 2020) and indicates that the three-parameter power-law model adequately captures the dominant physical influences on transmission without overfitting.

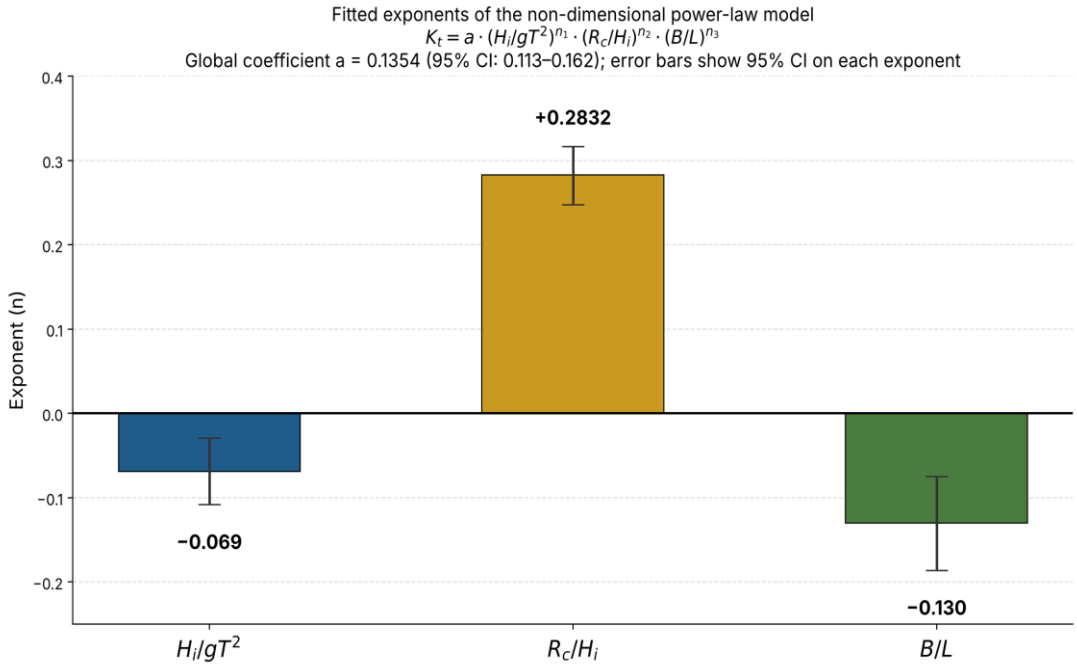


Figure 5: *Bar chart of the fitted exponents of the power-law model for each non-dimensional parameter governing Kt in the ARB-2 submerged breakwater. Error bars show 95% confidence intervals; the global coefficient is a = 0.1354 (95% CI: 0.113–0.162). Source: authors' elaboration based on power-law regression of experimental data.*

Slika 5: *Stolpični diagram prilagojenih eksponentov potenčnega modela za vsak brezdimenzijski parameter, ki vpliva na Kt v potopljenem valobranu ARB-2. Navpične črte prikazujejo 95-odstotne intervale zaupanja; globalni koeficient je a = 0,1354 (95-odstotni IZ: 0,113–0,162).*

4.6 Practical Implications and Ecological Compatibility

The experimental findings have direct practical implications for the design and deployment of ARB-2 as a coastal protection solution. The measured *Kt* range of 0.175–0.469 indicates that ARB-2 configurations can reduce transmitted wave heights by 53–82% relative to incident conditions, depending on the combination of structural geometry and prevailing wave climate. This performance range is sufficient to protect sandy and coral beaches from moderate wave energy impingement (Azima et al., 2023; Suprijo et al., 2024) and is competitive with conventional rubble-mound submerged breakwaters that require larger material volumes and construction footprints.

The modular, interlocking nature of ARB-2 provides additional practical advantages: units can be pre-fabricated, transported, and deployed with standard marine lifting equipment; the configuration can be adapted to varying water depths and coastal geometries; and the structure can be maintained or expanded incrementally without decommissioning the entire installation. From an ecological perspective, the cylindrical internal cavities of ARB-2 add internal void space and surface area beyond what a solid armor unit of equivalent external dimensions (e.g. a plain concrete cube) would provide. The substrate-complexity literature on reef and armor-unit design generally associates greater void space and micro-topographic variety with higher colonization potential for encrusting organisms and refugia for juvenile fish (Adi et al., 2020; Wahyudi et al., 2019). The present study did not include a direct ecological

comparison between ARB-2 and solid armor units under matched hydrodynamic and field conditions, so this expected advantage should be regarded as a design rationale supported by the general habitat-complexity literature rather than as an experimentally demonstrated result of this study; controlled colonization trials comparing ARB-2 against solid units of equivalent external geometry are recommended to confirm it.

5. Conclusion

This laboratory investigation of the ARB-2 submerged breakwater provides clear experimental evidence of its capacity to attenuate incident wave energy across a wide range of hydrodynamic conditions. The controlled wave flume experiments demonstrated that the structure consistently reduces transmitted wave heights, with transmission coefficients spanning 0.175 to 0.469, representing wave height reductions of 53% to 82% relative to incident conditions. The first research objective – experimental quantification of *Kt* for ARB-2 – is thus fully achieved.

Analysis of the non-dimensional parameter groups confirms that relative submergence (Rc/Hi) and relative crest width (B/L) are the dominant predictors of transmission performance, with exponents of +0.2832 and −0.130, respectively. Wave steepness (Hi/gT^2) exerts a comparatively minor influence under the tested conditions, reflected in its exponent of −0.069. The power-law regression model (equation (3)) with fitted coefficients provides predictions consistent with the measured dataset, satisfying the third objective of deriving a validated predictive model for engineering application.

The primary scientific contribution of this work is the first empirically validated, non-dimensionally parameterized characterization of wave transmission through the ARB-2 submerged breakwater, including defined applicability ranges for each non-dimensional variable. The findings close an identified gap in the coastal engineering literature regarding modular porous artificial reef units and provide a quantitative design basis for ARB-2 field deployment. Within the tested range, ARB-2 configurations achieved transmission coefficients (Kt = 0.175–0.469) comparable in magnitude to those reported for narrow-crested rubble-mound submerged breakwaters under regular waves (Kt = 0.36–0.99; Repousis et al., 2023), while additionally offering modular installation and, based on its porous concrete geometry, potential ecological habitat value. A direct side-by-side comparison under matched geometry and wave conditions was not performed and is recommended for future work.

The present study has several limitations that define the scope of the findings. Experiments were conducted using regular monochromatic waves in a two-dimensional flume, whereas natural coastal wave fields are irregular, multi-directional, and spectrally broad. Because of this, the reported Kt values and the fitted prediction equation should be regarded as applicable to regular-wave conditions; the results are qualitative indicators of ARB-2 performance rather than a validated design tool for irregular sea states, and physical or numerical testing under random waves is recommended before field application. The scale of the physical model imposes Reynolds number similarity constraints that may not fully replicate turbulent boundary layer behavior at prototype scale. Additionally, the ARB-2 configuration tested was fixed in a single stepped geometry; alternative assembly configurations and porosity arrangements may yield different performance characteristics. Seabed scour, biological fouling over time, and long-term structural settlement were not investigated.

Future research directions recommended on the basis of these findings include: (1) testing under irregular wave spectra using JONSWAP or Bretschneider spectral shapes to quantify performance under realistic sea states; (2) three-dimensional physical model experiments in a wave basin to evaluate transmission under oblique and multi-directional wave conditions; (3) numerical simulation of ARB-2 using volume-of-fluid or smoothed-particle hydrodynamics methods to resolve intra-cavity flow fields; (4) field-scale deployment and monitoring at an Indonesian coastal

site to validate laboratory scaling; and (5) optimization of the ARB-2 cavity geometry and porosity ratio using response surface methodology to identify configurations that maximize wave attenuation per unit structure volume.

Acknowledgments

The authors express their sincere gratitude to the Civil Engineering Study Program, Faculty of Engineering, Sultan Agung Islamic University (UNISSULA), Semarang, for providing laboratory facilities and institutional support throughout the research program. The authors also thank the technical staff of the hydraulics laboratory for their assistance in physical model construction and instrumentation.

CRediT authorship contribution statement

Andrew Ghea Mahardika: Conceptualization, Methodology, Formal Analysis, Investigation, Data Curation, Writing – Original Draft, Visualization.

S. Imam Wahyudi: Supervision, Conceptualization, Writing – Review & Editing, Resources, Validation.

Rachmat Mudiyono: Supervision, Project Administration, Writing – Review & Editing, Validation, Funding Acquisition.

Data availability

The experimental data supporting the findings of this study are openly available in the Zenodo repository under the dataset entitled "Experimental Dataset for Wave Transmission Performance of a Submerged Breakwater Constructed from Artificial Reef Brick-2 (ARB-2)" at https://doi.org/10.5281/zenodo.22688528. The deposited dataset contains 90 experimental runs representing 30 parameter sets, including the principal measured and derived variables used in the analyses presented in this article.

Declaration of interest

The authors declare no conflict of interest. No generative AI tools were used in the writing or preparation of this manuscript.

Funding

This research received no specific grant from any funding agency in the public, commercial, or not-for-profit sectors.

References

Adi, H. P., Wahyudi, S. I., Husni, F. (2020). Plastic barrels as platform material of floating house in coastal areas. IOP Conference Series: Earth and Environmental Science, **437**, 012006. https://doi.org/10.1088/1755-1315/437/1/012006.

Azima, F., Harmiyati, F. A., Muttaqin, M. Z. (2023). Evaluation of breakwater performance against waves at Tanjung Medang Beach. *Jurnal Saintis*, **23(1)**. https://doi.org/10.25299/saintis.2023.vol23(01).25225.

Calabrese, M., Vicinanza, D., Buccino, M. (2003). Large-scale experiments on the behaviour of low crested and submerged breakwaters in presence of broken waves. In: *Coastal Engineering* 2002, 1900-1912.

d'Angremond, K., van der Meer, J. W., de Jong, R. J. (1997). Wave transmission at low-crested structures. In: *Coastal Engineering* 1996, 2418-2427.

Goda, Y., Ahrens, J. P. (2009). New formulation of wave transmission over and through low-crested structures. In: *Coastal Engineering* 2008, 3530-3541.

Haz, A. A., Zakaria, A., Tugiono, S., Joko, D. (2022). Study of wave diffraction over submerged breakwaters with variation of wavelength. *Jurnal Rekayasa Sipil dan Desain*, **9(4)**, 933-942. https://doi.org/10.23960/jrsdd.v9i4.2207.

Huddiankuwera, A., Sitorus, P. H., Wibowo, R. A. (2024). Pengaruh parameter gelombang terhadap transmisi gelombang pada pemecah gelombang berongga tipe tenggelam (Influence of wave parameters on wave transmission in hollow submerged breakwaters). Konferensi Nasional Teknik Sipil (KoNTekS), **1(1)**. https://doi.org/10.62603/konteks.v1i1.10 (in Indonesian).

Kurdistani, S. M., Tomasicchio, G. R., D'Alessandro, F., Francone, A. (2022). Formula for wave transmission at submerged homogeneous porous breakwaters. *Ocean*

Engineering, **266**, 113053. https://doi.org/10.1016/j.oceaneng.2022.113053.

Magdalena, I., Atras, M. F., Sembiring, L., Nugroho, M. A., Labay, R. S. B., Roque, M. P. (2020). Wave transmission by rectangular submerged breakwaters. *Computation*, **8(2)**, 56. https://doi.org/10.3390/computation8020056.

Mahardika, A. G., Ramady, G. D. (2020). Pengaruh koefisien transmisi pada model pemecah gelombang tenggelam dengan armor artificial reef brick-1 (Influence of transmission coefficient on a submerged breakwater model with artificial reef brick-1 armor). *Jurnal Teknik Sipil Universitas Tanjungpura*, **20(2)**. https://doi.org/10.26418/jtst.v20i2.43550 (in Indonesian).

Min, E.-H., Koo, W., Kim, M.-H. (2023). Wave characteristics over a dual porous submerged breakwater using a fully nonlinear numerical wave tank with a porous domain. *Journal of Marine Science and Engineering*, **11(9)**, 1648. https://doi.org/10.3390/jmse11091648.

Rachmanda, F., Tugiono, S., Zakaria, A., Herison, A. (2022). Stability analysis of submerged rock breakwater. *Jurnal Rekayasa Sipil dan Desain*, **10(2)**, 385-394. https://doi.org/10.23960/jrsdd.v10i2.2621.

Repousis, E., Roupas, I., Memos, C. (2023). Wave transmission over rubble-mound submerged breakwaters. *Journal of Marine Science and Engineering*, **11(7)**, 1346. https://doi.org/10.3390/jmse11071346.

Rudan, S., Sviličić, Š. (2024). Determination of submerged breakwater efficiency using computational fluid dynamics. *Oceans*, **5(4)**, 742-757. https://doi.org/10.3390/oceans5040042.

Silva, R. F. da, Lowe, R. J., Hansen, J. E., Atkinson, A., Naderi, N. (2024). Wave basin experiments of wave-driven hydrodynamics over submerged coastal structures and artificial reefs. In: CoastLab 2024: *Physical Modelling in Coastal Engineering and Science*.

Suprijo, T., Napitupulu, G., Ginting, J. W. R., Abdullah, F. A. R., Khadami, F. (2024). Transformation of regular waves due to a two-row staggered pile breakwater. *Jurnal Teknik Hidraulik*, **15(2)**.

Tomasicchio, G. R., D'Alessandro, F. (2013). Wave energy transmission through and over low crested breakwaters. *Journal of Coastal Research*, **65**, 398-403.

van Gent, M. R. A., Buis, L., van den Bos, J. P., Wüthrich, D. (2023). Wave transmission at submerged coastal structures and artificial reefs. *Coastal Engineering*, **184**, 104344. https://doi.org/10.1016/j.coastaleng.2023.104344.

Wahyudi, S. I., Adi, H. P. (2018). Tidal flood handling through community participation in drainage management system. *International Journal of Integrated Engineering*, **10(2)**, 42-49.

Wahyudi, S. I., Adi, H. P., Husni, F. (2019). Wave simulation to compare existing and extended jetty in river estuary. *Advances in Engineering Research*, **190**, 137-143. https://doi.org/10.2991/aer.k.191110.023.

Wahyudi, S. I., Ni'am, M. F., Le Bras, G. (2012). Problems, causes and handling analysis of tidal flood, erosion and sedimentation in northern coast of Central Java: Review and recommendation. *International Journal of Civil & Environmental Engineering*, **12(4)**, 65-69.

Appendix A. Supplementary Figures

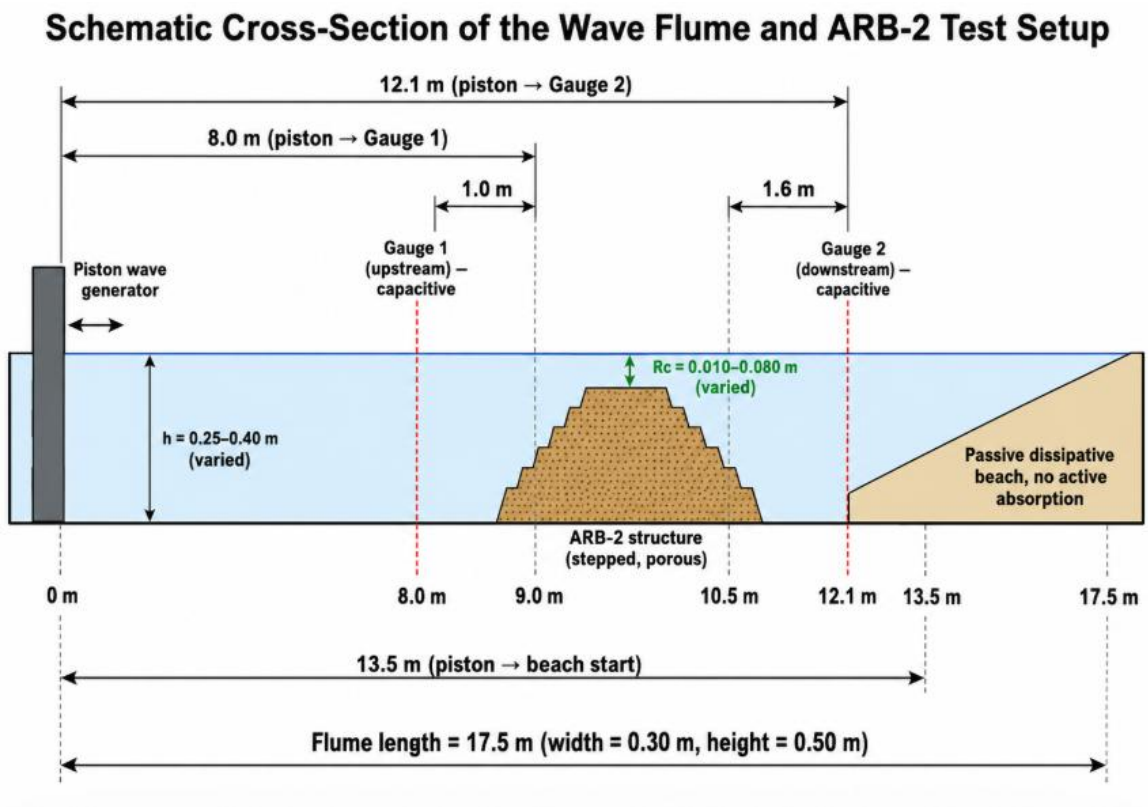


Figure A1: *Schematic cross-section of the wave flume and ARB-2 test setup. All dimension lines are anchored to fixed reference points (the piston face and the two capacitive wave gauges) and are drawn to match the distances reported in Section 3.2 (piston-to-Gauge 1 = 8.0 m; piston-to-Gauge 2 = 12.1 m; Gauge 1-to-structure toe = 1.0 m; structure toe-to-Gauge 2 = 1.6 m). Crest submergence depth (Rc) and water depth (h) are also indicated. Structure geometry is shown schematically; not to scale.*

Slika A1: *Shematski prečni prerez valovnega kanala in eksperimentalne postavitve ARB-2. Vse kotirne črte so vezane na fiksne referenčne točke (čelo bata ter oba kapacitivna merilnika valov) in so narisane skladno z razdaljami, navedenimi v poglavju 3.2 (bat do merilnika 1 = 8,0 m; bat do merilnika 2 = 12,1 m; merilnik 1 do vznožja konstrukcije = 1,0 m; vznožje konstrukcije do merilnika 2 = 1,6 m). Prikazani sta tudi globina potopitve grebena (Rc) in globina vode (h). Geometrija konstrukcije je prikazana shematsko in ni v merilu.*

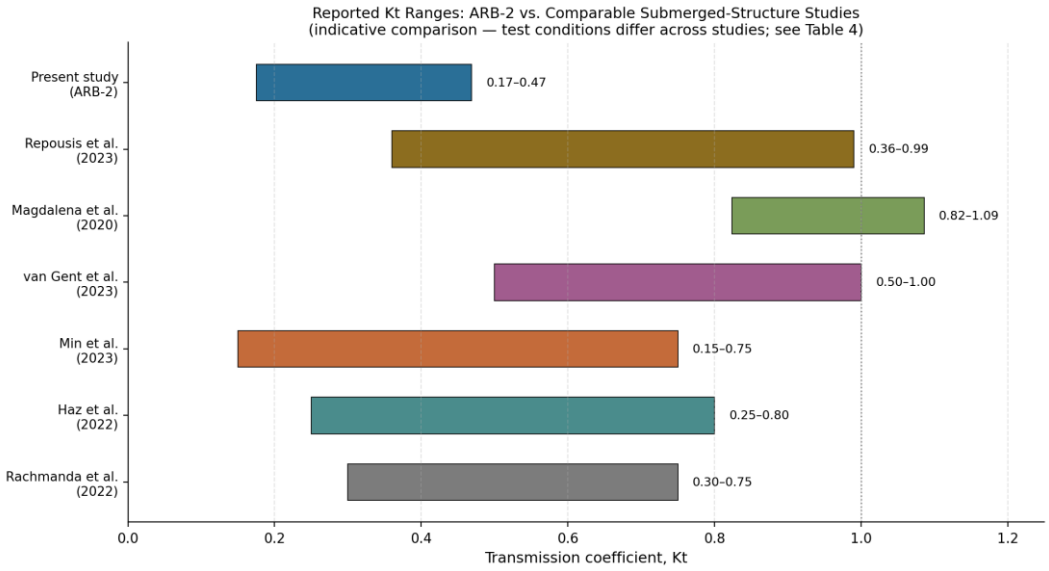


Figure A2: *Reported Kt ranges for ARB-2 and comparable submerged-structure studies from Table 4. Test conditions differ across studies; comparison is indicative.*

Slika A2: *Poročani razponi Kt za ARB-2 in primerljive študije potopljenih objektov iz preglednice 4. Preskusni pogoji se med študijami razlikujejo; primerjava je zgolj okvirna.*

Appendix B. Full Experimental Dataset (90 Runs)

Table A1 lists all 90 individual test runs (30 parameter sets × 3 repeats), giving the incident wave height, wave period, water depth, crest submergence depth, crest width, and measured transmission coefficient for each run.

Preglednica A1 podaja vseh 90 preizkusov (30 naborov parametrov × 3 ponovitve), pri čemer so za vsak preizkus podani višina vpadnega vala, perioda vala, globina vode, globina potopitve grebena, širina grebena in izmerjeni koeficient prepustnosti.

Run	Set	Hi (m)	T (s)	h (m)	Rc (m)	B (m)	Kt
1	1	0.0990	1.00	0.25	0.0383	0.35	0.1801
2	1	0.1000	1.00	0.25	0.0383	0.35	0.1750
3	1	0.0995	1.00	0.25	0.0383	0.35	0.1822
4	2	0.0300	2.50	0.40	0.0800	0.20	0.4408
5	2	0.0302	2.50	0.40	0.0800	0.20	0.4322
6	2	0.0304	2.50	0.40	0.0800	0.20	0.4241
7	3	0.0300	1.40	0.25	0.0100	0.35	0.1864
8	3	0.0302	1.40	0.25	0.0100	0.35	0.1790
9	3	0.0301	1.40	0.25	0.0100	0.35	0.2194
10	4	0.0797	2.00	0.35	0.0600	0.20	0.2521
11	4	0.0807	2.00	0.35	0.0600	0.20	0.2674
12	4	0.0794	2.00	0.35	0.0600	0.20	0.2975
13	5	0.0972	1.56	0.30	0.0800	0.30	0.2531
14	5	0.0972	1.56	0.30	0.0800	0.30	0.2517
15	5	0.0975	1.56	0.30	0.0800	0.30	0.2345
16	6	0.0806	1.37	0.36	0.0800	0.25	0.2898
17	6	0.0804	1.37	0.36	0.0800	0.25	0.2985
18	6	0.0805	1.37	0.36	0.0800	0.25	0.2530
19	7	0.0488	1.54	0.37	0.0529	0.24	0.2953
20	7	0.0486	1.54	0.37	0.0529	0.24	0.3193
21	7	0.0490	1.54	0.37	0.0529	0.24	0.2982
22	8	0.0572	1.45	0.35	0.0800	0.27	0.2999
23	8	0.0574	1.45	0.35	0.0800	0.27	0.2557
24	8	0.0570	1.45	0.35	0.0800	0.27	0.3203
25	9	0.0837	2.31	0.31	0.0371	0.27	0.2380
26	9	0.0834	2.31	0.31	0.0371	0.27	0.1959
27	9	0.0835	2.31	0.31	0.0371	0.27	0.2336
28	10	0.0507	1.00	0.40	0.0621	0.26	0.2607
29	10	0.0505	1.00	0.40	0.0621	0.26	0.2714
30	10	0.0511	1.00	0.40	0.0621	0.26	0.2376
31	11	0.0938	1.33	0.32	0.0800	0.23	0.2394
32	11	0.0937	1.33	0.32	0.0800	0.23	0.2274
33	11	0.0941	1.33	0.32	0.0800	0.23	0.2407
34	12	0.0314	2.30	0.29	0.0499	0.21	0.4690
35	12	0.0315	2.30	0.29	0.0499	0.21	0.3767
36	12	0.0311	2.30	0.29	0.0499	0.21	0.3829
37	13	0.0369	1.08	0.32	0.0480	0.33	0.2671
38	13	0.0366	1.08	0.32	0.0480	0.33	0.2582

39	13	0.0367	1.08	0.32	0.0480	0.33	0.2767
40	14	0.0637	1.24	0.33	0.0800	0.20	0.2535
41	14	0.0639	1.24	0.33	0.0800	0.20	0.3155
42	14	0.0643	1.24	0.33	0.0800	0.20	0.2795
43	15	0.0984	2.21	0.29	0.0800	0.26	0.2813
44	15	0.0997	2.21	0.29	0.0800	0.26	0.2806
45	15	0.0986	2.21	0.29	0.0800	0.26	0.2433
46	16	0.0862	1.94	0.33	0.0800	0.30	0.2395
47	16	0.0862	1.94	0.33	0.0800	0.30	0.2740
48	16	0.0859	1.94	0.33	0.0800	0.30	0.2661
49	17	0.0425	2.08	0.26	0.0800	0.31	0.3458
50	17	0.0429	2.08	0.26	0.0800	0.31	0.3243
51	17	0.0428	2.08	0.26	0.0800	0.31	0.3619
52	18	0.0452	1.73	0.37	0.0800	0.31	0.3401
53	18	0.0454	1.73	0.37	0.0800	0.31	0.3242
54	18	0.0449	1.73	0.37	0.0800	0.31	0.3245
55	19	0.0832	2.10	0.26	0.0800	0.32	0.2671
56	19	0.0833	2.10	0.26	0.0800	0.32	0.2935
57	19	0.0826	2.10	0.26	0.0800	0.32	0.2526
58	20	0.0658	1.98	0.31	0.0800	0.24	0.3292
59	20	0.0660	1.98	0.31	0.0800	0.24	0.3234
60	20	0.0661	1.98	0.31	0.0800	0.24	0.2728
61	21	0.0556	1.26	0.25	0.0417	0.28	0.2229
62	21	0.0562	1.26	0.25	0.0417	0.28	0.2152
63	21	0.0556	1.26	0.25	0.0417	0.28	0.2180
64	22	0.0945	2.17	0.36	0.0800	0.22	0.2896
65	22	0.0928	2.17	0.36	0.0800	0.22	0.3144
66	22	0.0931	2.17	0.36	0.0800	0.22	0.3302
67	23	0.0400	1.12	0.27	0.0333	0.28	0.2443
68	23	0.0407	1.12	0.27	0.0333	0.28	0.2123
69	23	0.0403	1.12	0.27	0.0333	0.28	0.2375
70	24	0.0769	1.88	0.34	0.0428	0.29	0.2374
71	24	0.0781	1.88	0.34	0.0428	0.29	0.2740
72	24	0.0770	1.88	0.34	0.0428	0.29	0.2266
73	25	0.0593	1.84	0.28	0.0385	0.25	0.2225
74	25	0.0586	1.84	0.28	0.0385	0.25	0.2638
75	25	0.0591	1.84	0.28	0.0385	0.25	0.2430
76	26	0.0392	1.48	0.27	0.0800	0.33	0.2988
77	26	0.0391	1.48	0.27	0.0800	0.33	0.3210

78	26	0.0394	1.48	0.27	0.0800	0.33	0.3272
79	27	0.0608	2.35	0.39	0.0377	0.35	0.2835
80	27	0.0601	2.35	0.39	0.0377	0.35	0.3158
81	27	0.0614	2.35	0.39	0.0377	0.35	0.2354
82	28	0.0510	2.04	0.38	0.0179	0.21	0.2347
83	28	0.0513	2.04	0.38	0.0179	0.21	0.2203
84	28	0.0507	2.04	0.38	0.0179	0.21	0.2436
85	29	0.0676	1.77	0.35	0.0800	0.29	0.3161
86	29	0.0673	1.77	0.35	0.0800	0.29	0.2851
87	29	0.0668	1.77	0.35	0.0800	0.29	0.3374
88	30	0.0340	1.65	0.38	0.0673	0.32	0.3877
89	30	0.0340	1.65	0.38	0.0673	0.32	0.3463
90	30	0.0338	1.65	0.38	0.0673	0.32	0.3678